Biophysical Letter

Mapping the Processivity Determinants of the Kinesin-3 Motor Domain

Guido Scarabelli,[1] Virupakshi Soppina,[2] Xin-Qiu Yao,[1] Joseph Atherton,[3] Carolyn A. Moores,[3] Kristen J. Verhey,[2,*] and Barry J. Grant[1,*]

[1]Department of Computational Medicine and Bioinformatics and [2]Department of Cell and Developmental Biology, University of Michigan Medical School, Ann Arbor, Michigan; and [3]Institute of Structural and Molecular Biology, Birkbeck College, University of London, London, United Kingdom

ABSTRACT Kinesin superfamily members play important roles in many diverse cellular processes, including cell motility, cell division, intracellular transport, and regulation of the microtubule cytoskeleton. How the properties of the family-defining motor domain of distinct kinesins are tailored to their different cellular roles remains largely unknown. Here, we employed molecular-dynamics simulations coupled with energetic calculations to infer the family-specific interactions of kinesin-1 and kinesin-3 motor domains with microtubules in different nucleotide states. We then used experimental mutagenesis and single-molecule motility assays to further assess the predicted residue-wise determinants of distinct kinesin-microtubule binding properties. Collectively, our results identify residues in the L8, L11, and α6 regions that contribute to family-specific microtubule interactions and whose mutation affects motor-microtubule complex stability and processive motility (the ability of an individual motor to take multiple steps along its microtubule filament). In particular, substitutions of prominent kinesin-3 residues with those found in kinesin-1, namely, R167S/H171D, K266D, and R346M, were found to decrease kinesin-3 processivity 10-fold and thus approach kinesin-1 levels.

Received for publication 22 June 2015 and in final form 20 August 2015.

*Correspondence: kjverhey@umich.edu or bjgrant@umich.edu

Guido Scarabelli and Virupakshi Soppina contributed equally to this work.

Kinesins are a large superfamily of microtubule-based motor proteins, with individual family members playing essential roles in cell division, cell motility, and intracellular trafficking. All kinesins contain a family-defining motor domain that enables nucleotide-dependent interactions with the microtubule lattice. General principles of how kinesin motor domains interact with nucleotide and microtubules have been established based on extensive biochemical and biophysical studies of kinesin-1. In particular, it has been demonstrated that alternating ATP binding and hydrolysis in each kinesin-1 motor domain leads to coordinated changes in microtubule binding affinity that enable processive motility (the ability to undergo many steps along the microtubule surface without dissociating) (1,2). It has been assumed that this is the mechanistic paradigm for all kinesin motors. However, recent work indicates that some kinesin motors utilize their core motor domain for very different functions. For example, the kinesin-8 and kinesin-13 families depolymerize microtubules (3,4). Even for the conventional property of processive motility, evolutionary tuning of the core motor domain has resulted in a range of family-specific processivities. For example, some kinesin-4 motors are nonprocessive (5), whereas kinesin-3 motors are superprocessive, being 10-fold more processive than kinesin-1 (6). How sequence divergence within the motor domain gave rise to these different properties remains an outstanding question in the field of cellular and molecular biology.

To identify microtubule interactions that contribute to family-specific motility properties, we utilized our recent cryo-electron microscopy structures of kinesin-3 and kinesin-1 on microtubules (7) and employed molecular-dynamics simulations and energetic calculations. We then used experimental mutagenesis and single-molecule motility assays to assess the predicted determinants of their distinct microtubule binding properties.

Kinesin-3 displays more extensive microtubule interactions than kinesin-1

Molecular-dynamics simulations and molecular mechanics with generalized Born and surface area solvation (MM/GBSA) binding energy calculations indicate that the residues that contribute to motor-microtubule stability are clustered in

Editor: E. Michael Ostap.

http://dx.doi.org/10.1016/j.bpj.2015.08.027

the same six regions (L2, L7, L8, L11-α4, L12, and α6) on the surface of the kinesin-1 and kinesin-3 motor domains (Fig. 1, *A* and *B*, and Figs. S1–S3 in the Supporting Material). In general, kinesin-3 was found to exhibit more extensive interactions with the tubulin surface than kinesin-1 (Fig. 1 *B*). The L2 region makes a comparatively minor contribution to the tubulin binding of both kinesin-1 and kinesin-3 (Figs. S2 and S3), despite the presence of a family-specific seven-amino-acid insertion in this region of kinesin-3 motors (Fig. S4). The L7 region also makes comparatively minor energetic contributions to complex stability for both kinesin-1 and kinesin-3 (Figs. 1 *B*, S2, and S3). By contrast, the L8 region provides a larger contribution due to extensive contacts with the H12 region of β-tubulin. Particularly notable are the strong electrostatic contributions from the kinesin-3 residues R167 and R169 in all nucleotide states. Kinesin-1 lacks direct equivalents of these charged residues and instead coordinates with the microtubule via R161 in the Apo state and K166 in the ADP state (Figs. S2 and S3).

Different charge distributions and energetic contributions are also evident for the L11-α4, L12, and α6 regions. For L11-α4, both motors display extensive interactions and high binding energies with the microtubule surface. Notable are R254, K261, and K266 of kinesin-3, which display strong interactions with tubulin in the ATP and Apo states but weaker interactions in the ADP state (Figs. 1 *B* and S3), as well as the interactions of K237 of kinesin-1 in both the Apo and ATP states and K252 in the ADP state (Fig. S2). The L12 region also contributes strong interactions with tubulin in both motors. Particularly notable is residue R307 in kinesin-3 and the equivalent R278 in kinesin-1 (Figs. S2 and S3). Finally, strong interactions of the α6 helix with tubulin can be observed for kinesin-3 and originate from residues R346 and R350 in all nucleotide states (Figs. 1 *B* and S3). However, the α6 region of kinesin-1 displays a different pattern of exposed charges and makes comparatively minor energetic contributions through residues K313 and R321 (Figs. 1 *B* and S2).

Collectively, this analysis identified differences between kinesin-1 and kinesin-3 motors in the extent of their microtubule interactions and binding energies (see the distinct kinesin-3 and kinesin-1 peaks in Figs. 1 *B* and S5). We hypothesized that these differences contribute to distinct stabilities for each motor-microtubule complex that in turn determine the distinct motile properties of these motors. To test this hypothesis, we replaced kinesin-3 residues with the corresponding kinesin-1 amino acids (Figs. S4 and S5) and examined the effects on the energetics of motor-tubulin interactions computationally and on motility properties experimentally in single-molecule assays. For this analysis, we focused on the L2, L8, L11, and α6 regions, as L7 was predicted to contribute little to motor-microtubule

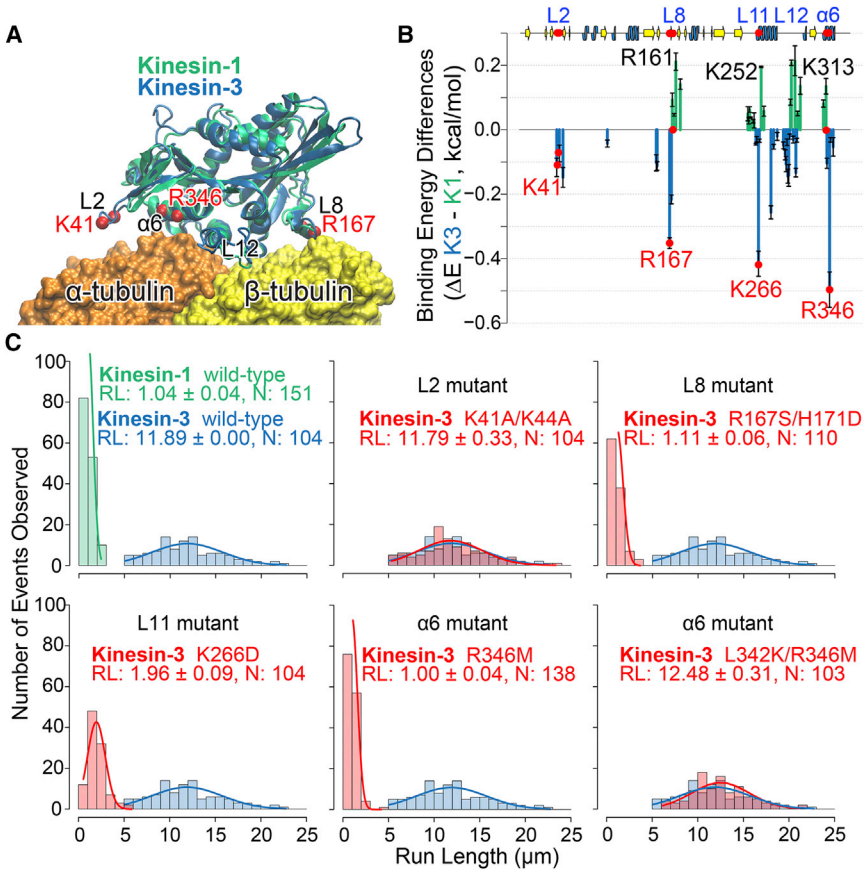

FIGURE 1 Altering select family-specific tubulin interactions of kinesin-3 motors reduces processivity. (*A*) Refined molecular structures for kinesin-1 (*green*) and kinesin-3 (*blue*) resulting from cryo-electron microscopy (7) and subsequent molecular-dynamics simulations (see Supporting Materials and Methods for full details). (*B*) Differences in the residue contribution to the binding energy for kinesin-1 (*green*) and kinesin-3 (*blue*) in the ATP state. These values were determined from four replicate 40-ns molecular-dynamics simulations and subsequent energetic calculations. Note that specific interactions of the L2, L7, L8, L11, and α6 regions are predicted to enhance the binding affinity of kinesin-3 in relation to kinesin-1. (*C*) Processivity measurements from single-molecule motility assays of wild-type kinesin-1 (*green*), wild-type kinesin-3 (*blue*), and kinesin-3 mutants (*red*). The average run length (RL) and number of observations (*N*) are noted.

stability (see above) and L12 was demonstrated in both Brownian dynamics simulations (8) and experimental work (9) to enhance the association kinetics of kinesin-3 motors with the microtubule rather than the processivity. Intriguingly, the results presented here indicate that the family-specific K-loop insertion in L12 of kinesin-3 motors lacks significant energetic interactions with tubulin (Fig. S3) and thus is predicted to have relatively little effect on motor-microtubule stability. L2 was included in this analysis despite its predicted minor contributions to tubulin binding energetics (Figs. 1 *B*, S2, and S3) due to its functional importance in other kinesin families (10).

Specific regions of the kinesin-3-microtubule interface contribute to interaction energy, velocity, and processivity

For L2, we replaced the two lysine residues at positions 41 and 44 with alanine residues to negate their electrostatic contributions to motor-microtubule stability. The resulting K41A/K44A mutant did not significantly alter the predicted binding affinity (ΔΔG 1.6 kcal/mol) and did not affect the experimentally determined velocity and run length values of the motor (2.13 ± 0.13 μm/s and 11.79 ± 0.33 μm, respectively; Figs. 1 *C*, S6, and S7). These results indicate that the L2 region is not a major determinant of distinct kinesin-3 motility properties.

We introduced mutations in the L8 region (R167S/H171D) to investigate the role of the predicted strong interactions of this region with the H12 region of β-tubulin. In the mutant Apo state, the missing wild-type interactions were predicted to be partially compensated for by R307 in L12, and by R346 and R350 in α6. These interactions result from a motor domain conformational rearrangement that positions α6 2.8 Å closer to the microtubule surface, leading to stronger interactions with α-tubulin H11 and H12 (Fig. S8) and an increased Apo-state binding affinity (ΔΔG −7.36 kcal/mol). In contrast, these new interactions were absent from the ATP state, which displayed an overall destabilization of the tubulin interface, resulting in a large reduction of the predicted binding affinity (ΔΔG 11.07 kcal/mol). The experimental motility assays for this mutant displayed reduced velocity and processivity values (1.32 ± 0.03 μm/s and 1.11 ± 0.06 μm; Fig. 1 *C*, S6, and S7). This result indicates that the identified residues in the L8 region of kinesin-3 contribute to the enhanced motility of wild-type kinesin-3.

The L11 region was also found to contribute to the enhanced stability of the kinesin-3/tubulin complex. In particular, the K266D mutation was observed to weaken tubulin interactions in both the ATP and Apo states (ΔΔG 6.66 and 7.58 kcal/mol, respectively) and resulted in a slower (1.68 ± 0.03 μm/s) and less processive (1.96 ± 0.09 μm) mutant motor (Figs. 1 *C*, S6, and S7). These results indicate that K266 in L11 is important for the enhanced processivity of kinesin-3.

Finally, we further investigated the potential family-specific interactions of the α6 region with tubulin via the single mutation R346M and double mutation L342K/R346M. For wild-type kinesin-3, R346 forms strong electrostatic interactions with the α-tubulin residues E415 and E421. Mutagenesis studies in budding yeast have suggested that both of these H12 α-tubulin residues are important for the interaction of kinesin proteins with microtubules (11). The R346M mutant removes the exposed positive charge on helix α6, and the double mutant L342K/R346M is predicted to retain a charge in this region complementary to that in kinesin-1 (on the next turn of the α6 helix; Fig. S1). Consistent with this energetic analysis, the R346M single mutant showed reduced velocity (1.19 ± 0.44 μm/s) and processivity (1.00 ± 0.04 μm), whereas the double mutant L342K/R346M displayed little variation in velocity (1.73 ± 0.01 μm/s) or processivity (12.48 ± 0.31 μm; Figs. 1, *B* and *C*, S6, and S7). These results highlight how analogous interactions can result from nonequivalent positions (i.e., nonaligned residues), indicating that one should consider multiple substitutions and potential epistatic effects when examining the collective determinants of enhanced kinesin-3 processivity.

In summary, using a combined computational and experimental approach, we have uncovered kinesin-3 family-specific tubulin interactions that influence motor-microtubule complex stability and motor processivity. Our results indicate that the family-specific distribution of exposed charges in L8, L11, and α6 regions result in distinct energetic interactions with the microtubule that affect kinesin motility. In particular, kinesin-3 R167 in L8, K266 in L11, and R346 in α6 contribute to the enhanced processivity of this motor in relation to kinesin-1, as their independent mutation resulted in a reduction of velocity and processivity. More broadly, these findings emphasize how processivity can be modulated by sequence differences intrinsic to individual motor domains in addition to established factors such as neck-linker composition (12–14). We suggest that our predictive approach should be widely applicable to additional families as well as to motor domain mutations linked to various diseases, including neurodegeneration and tumorigenesis. These expanded studies will generate new insights into how new motors can be custom engineered with distinctive motility properties.

SUPPORTING MATERIAL

Supporting Materials and Methods and eight figures are available at http://www.biophysj.org/biophysj/supplemental/S0006-3495(15)00862-0.

AUTHOR CONTRIBUTIONS

B.J.G., K.J.V., and C.A.M. designed the study. G.S., V.S., X.-Q.Y., B.J.G., and J.A. performed the research. G.S., B.J.G., K.J.V., and C.A.M. wrote the manuscript.

ACKNOWLEDGMENTS

We thank Dr. Rob Cross for valuable discussions.

This work was supported by the University of Michigan, the Medical Research Council (MR/J000973/1 to J.A. and C.A.M.), and the National Institutes of Health (R01070862 to K.J.V.).

REFERENCES

1. Svoboda, K., and S. M. Block. 1994. Force and velocity measured for single kinesin molecules. *Cell.* 77:773–784.
2. Toprak, E., A. Yildiz, …, P. R. Selvin. 2009. Why kinesin is so processive. *Proc. Natl. Acad. Sci. USA.* 106:12717–12722.
3. Tanenbaum, M. E., L. Macurek, …, R. H. Medema. 2011. A complex of Kif18b and MCAK promotes microtubule depolymerization and is negatively regulated by Aurora kinases. *Curr. Biol.* 21:1356–1365.
4. Hunter, A. W., M. Caplow, …, J. Howard. 2003. The kinesin-related protein MCAK is a microtubule depolymerase that forms an ATP-hydrolyzing complex at microtubule ends. *Mol. Cell.* 11:445–457.
5. Bringmann, H., G. Skiniotis, …, T. Surrey. 2004. A kinesin-like motor inhibits microtubule dynamic instability. *Science.* 303:1519–1522.
6. Soppina, V., S. R. Norris, …, K. J. Verhey. 2014. Dimerization of mammalian kinesin-3 motors results in superprocessive motion. *Proc. Natl. Acad. Sci. USA.* 111:5562–5567.
7. Atherton, J., I. Farabella, …, C. A. Moores. 2014. Conserved mechanisms of microtubule-stimulated ADP release, ATP binding, and force generation in transport kinesins. *eLife.* 3:e03680.
8. Grant, B. J., D. M. Gheorghe, …, R. A. Cross. 2011. Electrostatically biased binding of kinesin to microtubules. *PLoS Biol.* 9: e1001207.
9. Soppina, V., and K. J. Verhey. 2014. The family-specific K-loop influences the microtubule on-rate but not the superprocessivity of kinesin-3 motors. *Mol. Biol. Cell.* 25:2161–2170.
10. Kim, H., C. Fonseca, and J. Stumpff. 2014. A unique kinesin-8 surface loop provides specificity for chromosome alignment. *Mol. Biol. Cell.* 25:3319–3329.
11. Uchimura, S., Y. Oguchi, …, E. Muto. 2010. Key residues on microtubule responsible for activation of kinesin ATPase. *EMBO J.* 29:1167–1175.
12. Shastry, S., and W. O. Hancock. 2010. Neck linker length determines the degree of processivity in kinesin-1 and kinesin-2 motors. *Curr. Biol.* 20:939–943.
13. Andreasson, J. O., B. Milic, …, S. M. Block. 2015. Examining kinesin processivity within a general gating framework. *elife.* 4:e07403.
14. Milic, B., J. O. Andreasson, …, S. M. Block. 2014. Kinesin processivity is gated by phosphate release. *Proc. Natl. Acad. Sci. USA.* 111: 14136–14140.

Supporting Material

Mapping the processivity determinants of the kinesin-3 motor domain

Guido Scarabelli,[1] Virupakshi Soppina,[2] Xin-Qiu Yao,[1] Joseph Atherton,[3] Carolyn A. Moores,[3] Kristen Verhey,[2,*] and Barry J. Grant[1,*]

[1]Department of Computational Medicine and Bioinformatics, and [2]Department of Cell and Developmental Biology, University of Michigan Medical School, MI, USA. [3]Institute of Structural and Molecular Biology, Birkbeck College, University of London, UK

*Correspondence to K.V. kjverhey@umich.edu and B. J. G. bjgrant@umich.edu

Materials and methods

Molecular dynamics simulations

Simulation models were based on the crystallographic structures of human kinesin-1 in complex with the microtubule in the ATP and Apo states (PDB codes 4HNA and 4LNU) (1) (2) and on the CryoEM structures for human kinesin-3 in ATP, Apo and ADP states (PDB codes 4UXP, 4UXO, 4XUS) (3). The kinesin-1 ADP state complex was built from initially merging a kinesin-1 ADP state structure (PDB code 1BG2) with tubulin from a kinesin-3 ADP complex structure (PDB code 4XUS) via superposition based on the α4 helix (residues 255-270 in kinesin-1 and 278-293 in kinesin-3). A loop refinement optimization was performed on the kinesin-1 ADP state complex with Modeller v9.10 (4) for L8c segment (residues 158-162), L11 (residues 237-253), L12 (residues 271-276) and the neck-linker (residues 326-337) and evaluated using the discrete optimized protein energy score (5). All kinesin-tubulin model structures were built with the AMBER 12 package (6) and corresponding all-atom potential function ff99SB (7). Models were inserted in a cubic water box with margins located 12Å from the closest protein atom. The energetic parameters for the nucleotide molecules were obtained from the AMBER parameter database (8). TIP3P water molecules and sodium counter ions were added to each system. Four runs of energy minimization of 4000 cycles each were employed alternating every 100 cycle the steepest descent and the conjugate gradient algorithms. Positional restrains with a force of 500 kcal / (mol $Å^2$) were applied in the first run on all protein and ligand atoms. In the second run the restrains were applied on the protein backbone only and in the third run on the water and counter ions only. In the fourth run no atoms were restrained. A fifth energy minimization run of 4000 cycles was then performed using the conjugate gradient algorithm only and no atomic restrains. Two subsequent molecular dynamics runs of 10ps and 200ps were employed to increase each system temperature from 100K to 300K and to equilibrate each system configuration at 300K. The production runs started from these equilibrated conformations. Periodic boundary conditions and full particle-mesh Ewald electrostatics were used. A 12Å cutoff value was included for truncation of non-bonded interactions. The simulations were run at constant temperature (300 K) and constant pressure (1 atm) with a 2fs time step. The SHAKE algorithm was used to constrain all covalent bonds involving hydrogen atoms. Each simulation was 40ns long, and was reproduced four times with random initial velocity assignments, for a total of 160ns of production phase dynamics for each system.

MM/GBSA calculations

Molecular mechanics with generalized Born and surface area solvation (MM/GBSA) binding energy calculations were performed with the GB^{OBC} model (9) in AMBER 12 (6). For each simulated system, pairwise energy values (resulting from setting idecomp=4) were scaled by the average number of kinesin-microtubule interaction pairs in both in kinesin-1 and kinesin-3 (39 average contacts) and averaged over four replicate simulations. The total binding free energies reported in the main text were scaled by a factor of 0.3. This was obtained from linear fitting to experimental microtubule dissociation constants determined by Hirokawa and coworkers for kinesin-3 (10). Results obtained from the combined analysis of structural interactions across models of all nucleotide states of each kinesin were used to inform experiential site-directed mutagenesis studies. Residue level comparisons of kinesin-1 and kinesin-3 motor domains utilized a Bio3D structure based sequence alignment that mapped all equivalent (aligned) and non-equivalent (un-aligned) regions (11).

Site-directed mutagenesis

Mutations were introduced into plasmids encoding constitutively motile, dimeric versions of kinesin-3 KIF1A(1-393)LZ-3xmCitrine (12). All mutations were introduced using QuikChange site-directed mutagenesis (Agilent Technologies) and verified by DNA sequencing of both strands.

Cell Culture, Transfection and Cell Lysates

COS-7 (monkey kidney fibroblast, ATCC) cells were grown in DMEM + 10% (vol/vol) FBS and 2 mM L-glutamine at 37 °C with 5% (vol/vol) CO_2. Cells were transfected with 1.0 μg of plasmid DNA using Expressfect (Danville Scientific). After 16 hrs of transfection, the cell lysates were prepared as described previously (12). Briefly, COS-7 cells expressing fluorescent protein-tagged motors were trypsinized and pelleted by low-speed centrifugation at 4 °C. The pellet was washed once with cold DMEM culture medium and lysed in ice-cold lysis buffer (25 mM HEPES/KOH, 115 mM potassium acetate, 5 mM sodium acetate, 5 mM $MgCl_2$, 0.5 mM EGTA, and 1% Triton X-100, pH 7.4) freshly supplemented with 1 mM PMSF and protease inhibitors (10 μg/mL leupeptin, 5 μg/mL chymostatin, 3 μg/mL elastatinal, and 1 mg/mL pepstatin). The lysate was clarified by centrifugation at 16,000 × g at 4 °C and either used fresh for assays or aliquots were frozen in liquid nitrogen and stored at −80 °C until further use.

Microtubule polymerization

Microtubules were polymerized from purified tubulin (TL238, Cytoskeleton) in BRB80 buffer (80 mM Pipes/KOH pH 6.8, 1 mM $MgCl_2$, 1 mM EGTA) supplemented with 1mM GTP at 37 ^oC for 20 min, stabilized by addition of 5 volumes of pre-warmed BRB80 containing 20 μM taxol, incubated for 5 min, and then stored at room temperature.

Total Internal Reflection Fluorescence Single-Molecule Motility Assays

All single-molecule assays were performed at room temperature using a Nikon Ti-E objective-type total internal reflection fluorescence (TIRF) microscope with Perfect Focus System, a 100× 1.49 N.A. CFI APO TIRF objective, an Agilent 3-Line (488, 561, and 640 nm) Monolithic Standard Power Laser Launch with AOTF, an EMCCD camera (iXon+ DU897; Andor), and controlled by Nikon Elements image acquisition software. A narrow motility chamber (~10 μl volume) was assembled by attaching a clean #1.5 coverslip to a microscope slide with double-sided tape. Polymerized microtubules were diluted in P12 buffer (12 mM Pipes/KOH pH 6.8, 1 mM $MgCl_2$, 1 mM EGTA) containing 10 μM taxol and then introduced into the motility chamber and incubated for 5 min at room temperature to adsorb onto the coverslip. Subsequently, 50 μl of blocking buffer (10 mg/ml BSA in P12 buffer with 10 μM taxol) was introduced and incubated for 20 min to prevent non-specific binding of kinesin motors onto the coverslip surface. Finally, kinesin motors in a 50 μl Motility Mix (0.1 – 2.0 μl of COS-7 cell lysate with 30 μl of blocking buffer, 15 μl of P12 buffer, 2 mM ATP, 0.5 μl of 100 mM DTT, 0.5 μl of 100 mM $MgCl_2$, and 0.5 μl each of 20 mg/ml glucose oxidase, 8 mg/ml catalase and 1M glucose) was added to the flow chamber and the ends were sealed with molten paraffin wax and imaged at 10 frames/sec without binning and at low laser power to avoid photobleaching during processive motor runs.

Data Analysis

The position of fluorescent motor spots was manually tracked frame-by-frame using a custom-written plugin in ImageJ (nih.gov). The velocities and run lengths of individual motors were binned and histograms were generated for the population by plotting the number of events in each bin. The average velocity and run length were then obtained by fitting either a single Gaussian peak (velocity) or an exponential (run length) to the population histogram. The measurements for each construct come

from at least two independent protein preparations and include motile events lasting at least five frames (500 ms). All data are presented as mean ± standard error of mean (SEM).

Supporting References

1. Gigant, B., W. Wang, B. Dreier, Q. Jiang, L. Pecqueur, A. Pluckthun, C. Wang, and M. Knossow. 2013. Structure of a kinesin-tubulin complex and implications for kinesin motility. Nature Stru Mol Bio 20:1001-1007.
2. Cao, L., W. Wang, Q. Jiang, C. Wang, M. Knossow, and B. Gigant. 2014. The structure of apo-kinesin bound to tubulin links the nucleotide cycle to movement. Nature Commun 5:5364.
3. Atherton, J., I. Farabella, I. M. Yu, S. S. Rosenfeld, A. Houdusse, M. Topf, and C. A. Moores. 2014. Conserved mechanisms of microtubule-stimulated ADP release, ATP binding, and force generation in transport kinesins. eLife 3:e03680.
4. Sali, A., and T. L. Blundell. 1993. Comparative protein modelling by satisfaction of spatial restraints. J Mol Biol 234:779-815.
5. Shen, M. Y., and A. Sali. 2006. Statistical potential for assessment and prediction of protein structures. Prot Sci 15:2507-2524.
6. Case, D. A., T. A. Darden, T. E. I. Cheatham, T. E. Simmerling, J. Wang, R. E. Duke, R. Luo, R. C. Walker, W. Zhang, K. M. Merz, B. Roberts, S. Hayik, A. Roitberg, G. Seabra, J. Swails, A. W. Götz, I. Kolossváry, K. F. Wong, F. Paesani, J. Vanicek, R. M. Wolf, J. Liu, X. Wu, S. R. Brozell, T. Steinbrecher, H. Gohlke, Q. Cai, X. Ye, M.-J. Hsieh, G. Cui, D. R. Roe, D. H. Mathews, M. G. Seetin, R. Salomon-Ferrer, C. Sagui, V. Babin, T. Luchko, S. Gusarov, A. Kovalenko, and P. A. Kollman. 2012. AMBER 12. University of California, San Francisco.
7. Hornak, V., R. Abel, A. Okur, B. Strockbine, A. Roitberg, and C. Simmerling. 2006. Comparison of multiple Amber force fields and development of improved protein backbone parameters. Proteins 65:712-725.
8. Meagher, K. L., L. T. Redman, and H. A. Carlson. 2003. Development of polyphosphate parameters for use with the AMBER force field. J Comp Chem 24:1016-1025.
9. Onufriev, A., D. Bashford, and D. A. Case. 2004. Exploring protein native states and large-scale conformational changes with a modified generalized born model. Proteins 55:383-394.
10. Nitta, R., M. Kikkawa, Y. Okada, and N. Hirokawa. 2004. KIF1A alternately uses two loops to bind microtubules. Science 305:678-683.
11. Grant, B.J., Rodrigues, A. P. C., ElSawy, K. M., McCammon, J. A., & Caves, L. S. D. 2006. Bio3D: an R package for the comparative analysis of protein structures. Bioinformatics 22, 2695–2696.
12. Soppina, V., S. R. Norris, A. S. Dizaji, M. Kortus, S. Veatch, M. Peckham, and K. J. Verhey. 2014. Dimerization of mammalian kinesin-3 motors results in superprocessive motion. Proc Nat Acad Sci U S A 111:5562-5567.

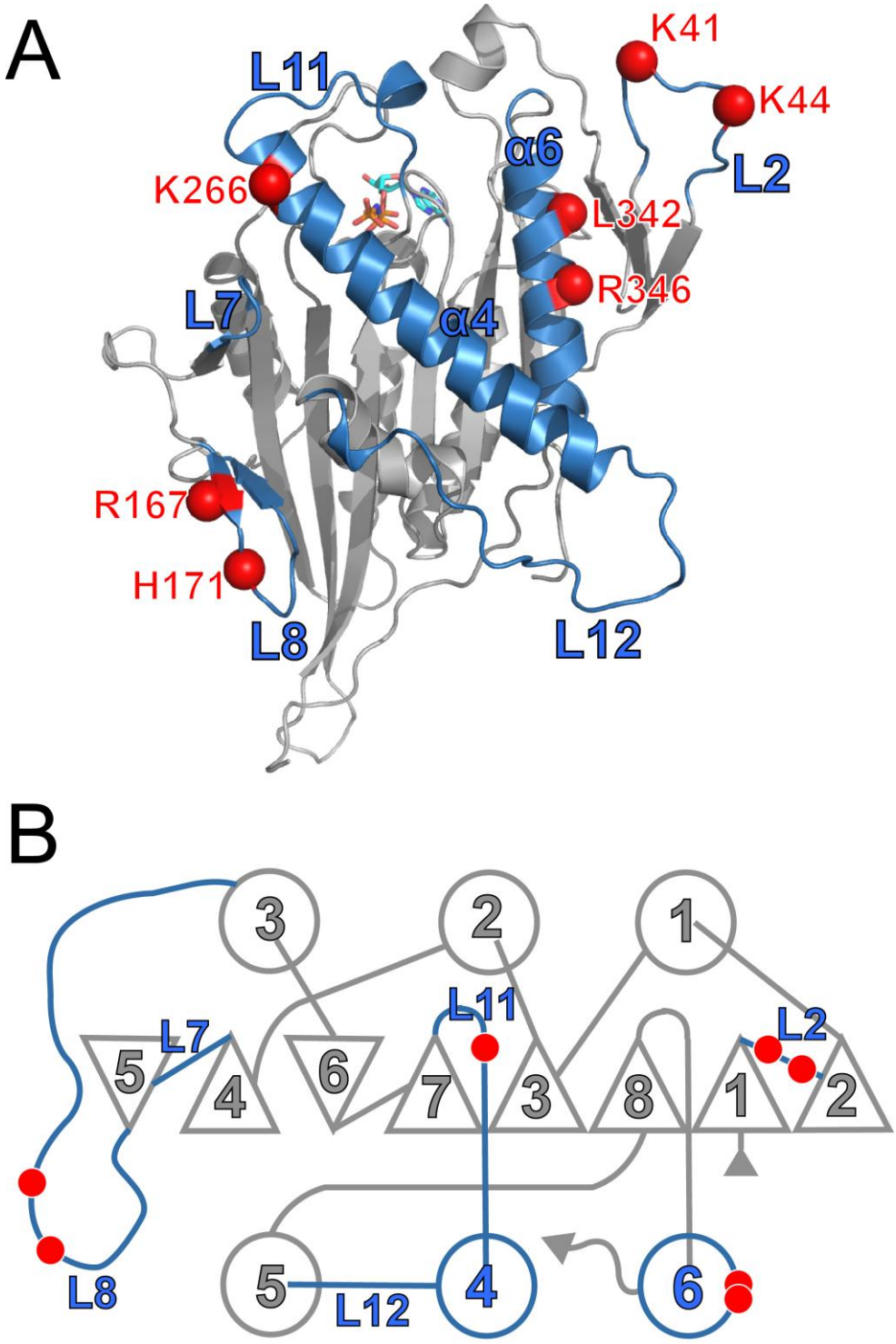

Figure S1. Kinesin-3 motor domain structure. (**A**) Kinesin regions displaying major energetic interactions with microtubule residues are rendered in blue. Red spheres indicate the location of mutation sites investigated in the current study. (**B**) Topological diagram of the kinesin-3 motor domain. Major β-strands are depicted as triangles and α-helices as circles. Regions are colored as in panel **A.**

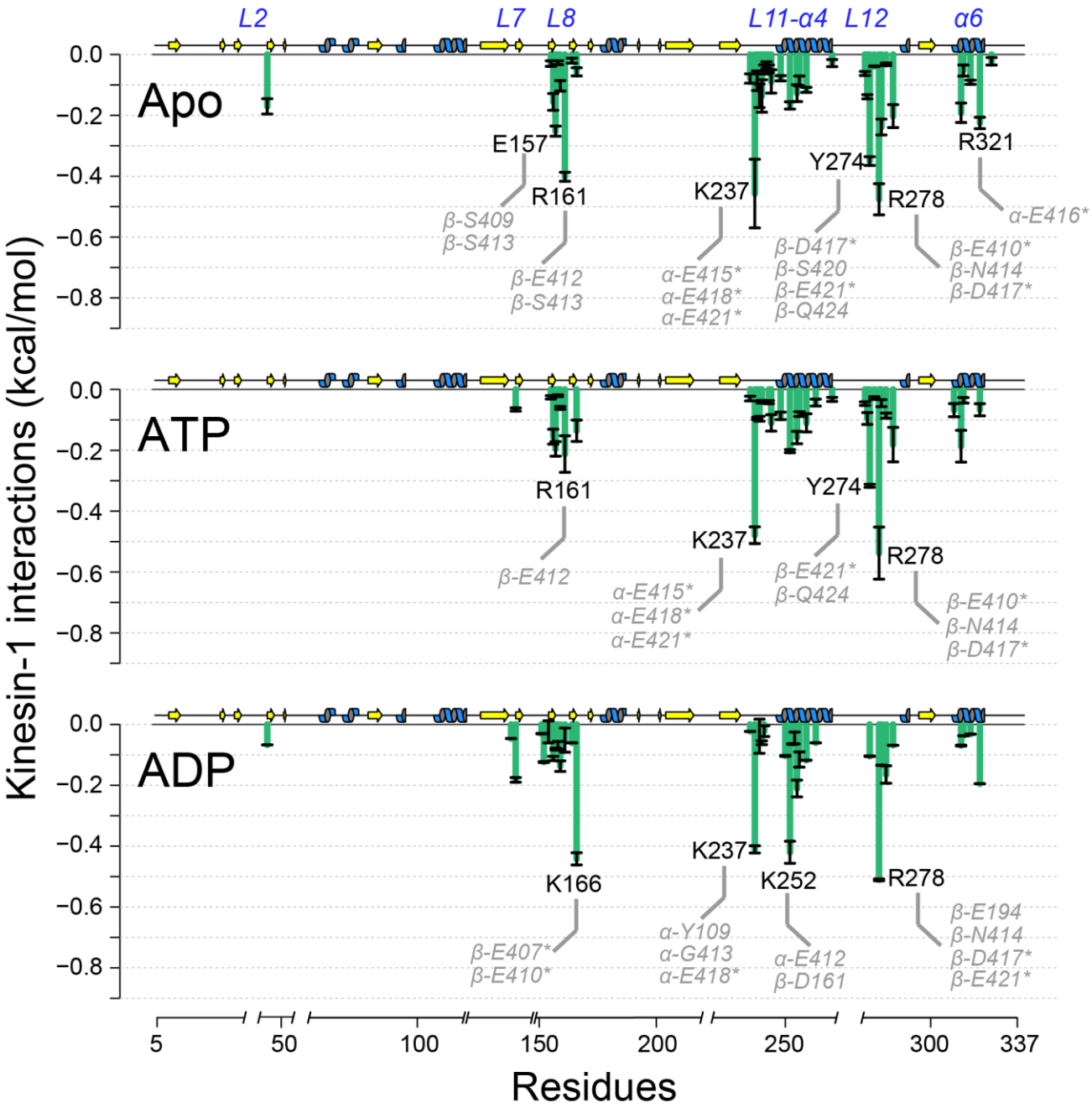

Figure S2. Kinesin-1 residue contributions to tubulin binding energy. Kinesin residues with prominent contributions are labeled in black and their major tubulin interacting partners are labeled in gray.

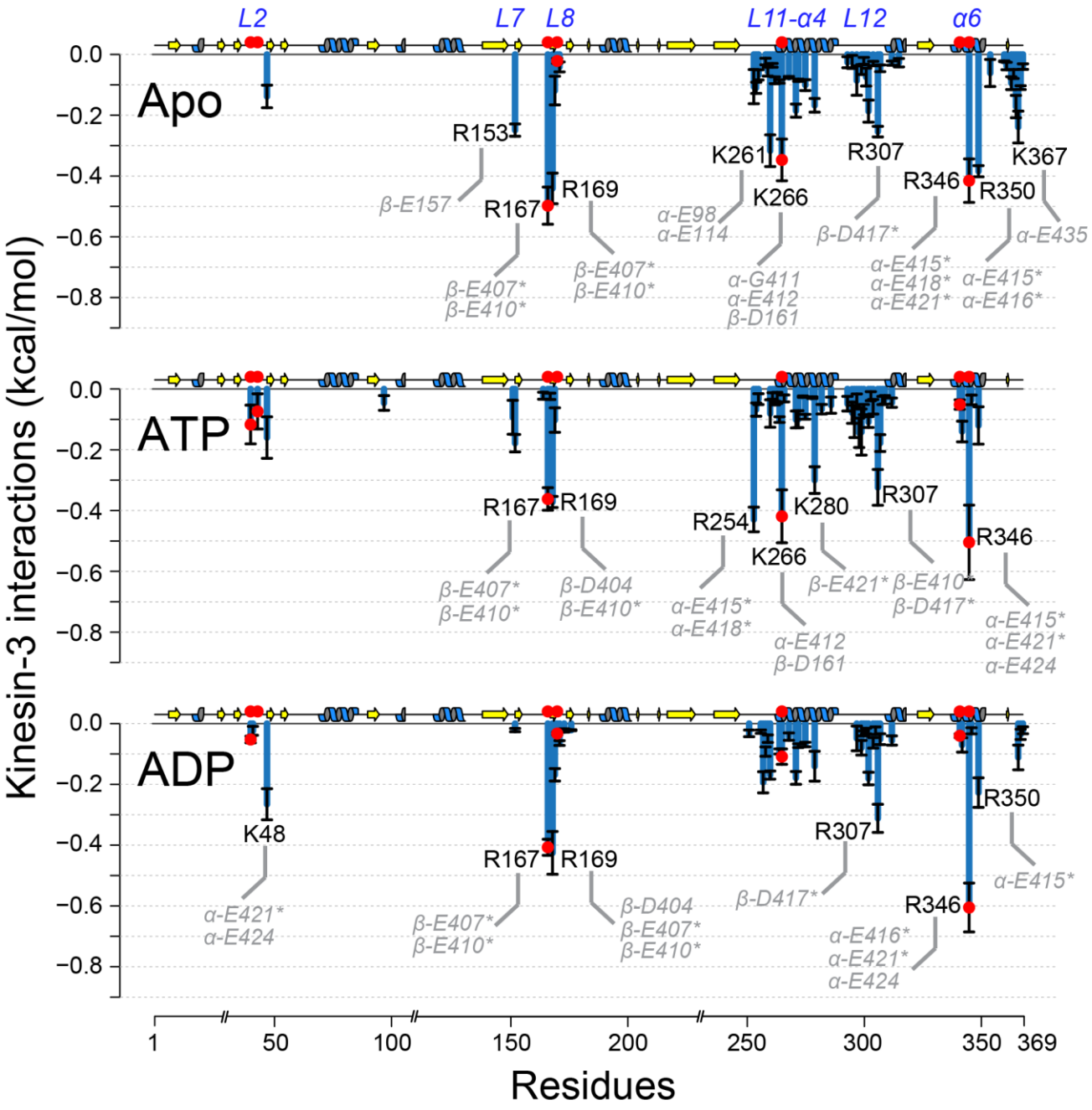

Figure S3. Kinesin-3 residue contributions to tubulin binding energy. Kinesin residues with prominent contributions are labeled in black and their major tubulin interacting partners are labeled in gray. The location of residues subjected to mutagenesis simulations and single molecule experiments are indicated with red points.

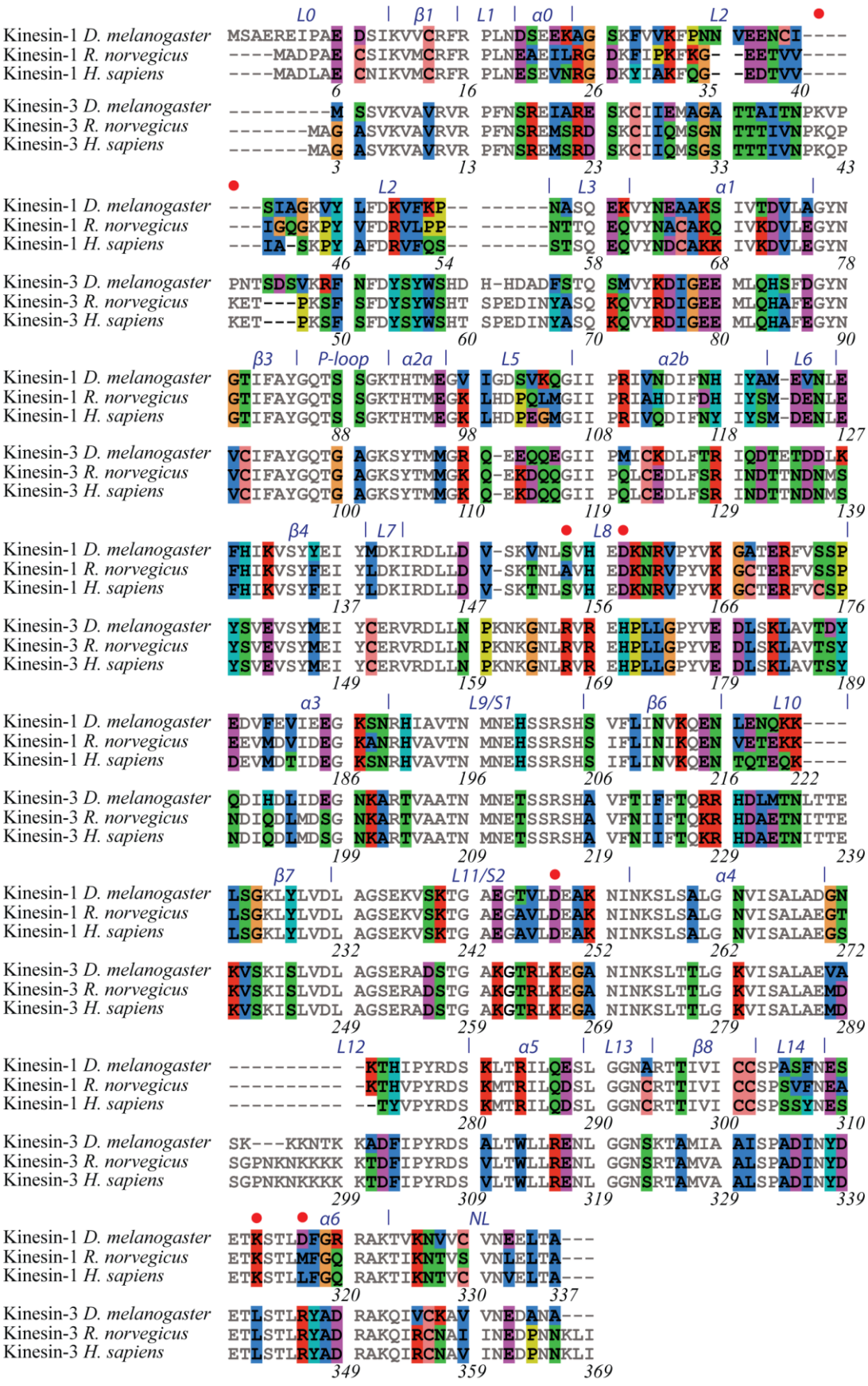
L0 β1 L1 α0 L2
Kinesin-1 D. melanogaster MSAEREIPAE DSIKVVCRFR PLNDSEEKAG SKFVVKFPNN VEENCI----
Kinesin-1 R. norvegicus ----MADPAE CSIKVMCRFR PLNEAEILRG DKFIPKFKG- -EETVV----
Kinesin-1 H. sapiens ----MADLAE CNIKVMCRFR PLNESEVNRG DKYIAKFQG- -EDTVV----
6 16 26 35 40
Kinesin-3 D. melanogaster ---------M SSVKVAVRVR PFNSREIARE SKCIIEMAGA TTAITNPKVP
Kinesin-3 R. norvegicus -------MAG ASVKVAVRVR PFNSREMSRD SKCIIQMSGN TTTIVNPKQP
Kinesin-3 H. sapiens -------MAG ASVKVAVRVR PFNSREMSRD SKCIIQMSGS TTTIVNPKQP
3 13 23 33 43
L2 L3 α1
Kinesin-1 D. melanogaster ---SIAGKVY LFDKVFKP-- ------NASQ EKVYNEAAKS IVTDVLAGYN
Kinesin-1 R. norvegicus ---IGQGKPY VFDRVLPP-- ------NTTQ EQVYNACAKQ IVKDVLEGYN
Kinesin-1 H. sapiens ---IA-SKPY AFDRVFQS-- ------STSQ EQVYNDCAKK IVKDVLEGYN
46 54 58 68 78
Kinesin-3 D. melanogaster PNTSDSVKRF NFDYSYWSHD H-HDADFSTQ SMVYKDIGEE MLQHSFDGYN
Kinesin-3 R. norvegicus KET---PKSF SFDYSYWSHT SPEDINYASQ KQVYRDIGEE MLQHAFEGYN
Kinesin-3 H. sapiens KET---PKSF SFDYSYWSHT SPEDINYASQ KQVYRDIGEE MLQHAFEGYN
50 60 70 80 90
β3 P-loop α2a L5 α2b L6
Kinesin-1 D. melanogaster GTIFAYGQTS SGKTHTMEGV IGDSVKQGII PRIVNDIFNH IYAM-EVNLE
Kinesin-1 R. norvegicus GTIFAYGQTS SGKTHTMEGK LHDPQLMGII PRIAHDIFDH IYSM-DENLE
Kinesin-1 H. sapiens GTIFAYGQTS SGKTHTMEGK LHDPEGMGII PRIVQDIFNY IYSM-DENLE
88 98 108 118 127
Kinesin-3 D. melanogaster VCIFAYGQTG AGKSYTMMGR Q-EEQQEGII PMICKDLFTR IQDTETDDLK
Kinesin-3 R. norvegicus VCIFAYGQTG AGKSYTMMGK Q-EKDQQGII PQLCEDLFSR INDTTNDNMS
Kinesin-3 H. sapiens VCIFAYGQTG AGKSYTMMGK Q-EKDQQGII PQLCEDLFSR INDTTNDNMS
100 110 119 129 139
β4 L7 L8
Kinesin-1 D. melanogaster FHIKVSYYEI YMDKIRDLLD V-SKVNLSVH EDKNRVPYVK GATERFVSSP
Kinesin-1 R. norvegicus FHIKVSYFEI YLDKIRDLLD V-SKTNLAVH EDKNRVPYVK GCTERFVSSP
Kinesin-1 H. sapiens FHIKVSYFEI YLDKIRDLLD V-SKTNLSVH EDKNRVPYVK GCTERFVCSP
137 147 156 166 176
Kinesin-3 D. melanogaster YSVEVSYMEI YCERVRDLLN PKNKGNLRVR EHPLLGPYVE DLSKLAVTDY
Kinesin-3 R. norvegicus YSVEVSYMEI YCERVRDLLN PKNKGNLRVR EHPLLGPYVE DLSKLAVTSY
Kinesin-3 H. sapiens YSVEVSYMEI YCERVRDLLN PKNKGNLRVR EHPLLGPYVE DLSKLAVTSY
149 159 169 179 189
α3 L9/S1 β6 L10
Kinesin-1 D. melanogaster EDVFEVIEEG KSNRHIAVTN MNEHSSRSHS VFLINVKQEN LENQKK----
Kinesin-1 R. norvegicus EEVMDVIDEG KANRHVAVTN MNEHSSRSHS IFLINIKQEN VETEKK----
Kinesin-1 H. sapiens DEVMDTIDEG KSNRHVAVTN MNEHSSRSHS IFLINVKQEN TQTEQK----
186 196 206 216 222
Kinesin-3 D. melanogaster QDIHDLIDEG NKARTVAATN MNETSSRSHA VFTIFFTQRR HDLMTNLTTE
Kinesin-3 R. norvegicus NDIQDLMDSG NKARTVAATN MNETSSRSHA VFNIIFTQKR HDAETNITTE
Kinesin-3 H. sapiens NDIQDLMDSG NKARTVAATN MNETSSRSHA VFNIIFTQKR HDAETNITTE
199 209 219 229 239
β7 L11/S2 α4
Kinesin-1 D. melanogaster LSGKLYLVDL AGSEKVSKTG AEGTVLDEAK NINKSLSALG NVISALADGN
Kinesin-1 R. norvegicus LSGKLYLVDL AGSEKVSKTG AEGAVLDEAK NINKSLSALG NVISALAEGT
Kinesin-1 H. sapiens LSGKLYLVDL AGSEKVSKTG AEGAVLDEAK NINKSLSALG NVISALAEGS
232 242 252 262 272
Kinesin-3 D. melanogaster KVSKISLVDL AGSERADSTG AKGTRLKEGA NINKSLTTLG KVISALAEVA
Kinesin-3 R. norvegicus KVSKISLVDL AGSERADSTG AKGTRLKEGA NINKSLTTLG KVISALAEMD
Kinesin-3 H. sapiens KVSKISLVDL AGSERADSTG AKGTRLKEGA NINKSLTTLG KVISALAEMD
249 259 269 279 289
L12 α5 L13 β8 L14
Kinesin-1 D. melanogaster ---------- -KTHIPYRDS KLTRILQESL GGNARTTIVI CCSPASFNES
Kinesin-1 R. norvegicus ---------- -KTHVPYRDS KMTRILQDSL GGNCRTTIVI CCSPSVFNEA
Kinesin-1 H. sapiens ---------- --TYVPYRDS KMTRILQDSL GGNCRTTIVI CCSPSSYNES
280 290 300 310
Kinesin-3 D. melanogaster SK---KKNTK KADFIPYRDS ALTWLLRENL GGNSKTAMIA AISPADINYD
Kinesin-3 R. norvegicus SGPNKNKKKK KTDFIPYRDS VLTWLLRENL GGNSRTAMVA ALSPADINYD
Kinesin-3 H. sapiens SGPNKNKKKK KTDFIPYRDS VLTWLLRENL GGNSRTAMVA ALSPADINYD
299 309 319 329 339
α6 NL
Kinesin-1 D. melanogaster ETKSTLDFGR RAKTVKNVVC VNEELTA---
Kinesin-1 R. norvegicus ETKSTLMFGQ RAKTIKNTVS VNLELTA---
Kinesin-1 H. sapiens ETKSTLLFGQ RAKTIKNTVC VNVELTA---
320 330 337
Kinesin-3 D. melanogaster ETLSTLRYAD RAKQIVCKAV VNEDANA---
Kinesin-3 R. norvegicus ETLSTLRYAD RAKQIRCNAI INEDPNNKLI
Kinesin-3 H. sapiens ETLSTLRYAD RAKQIRCNAV INEDPNNKLI
349 359 369

Figure S4. (Previous page). **Kinesin-1 and kinesin-3 structure based sequence alignment**. Residue numbers (black text) refer to Kinesin-1 and Kinesin-3 *H. sapiens*. Positions with divergent residue types are colored by their physiochemical properties (red positively charged; purple negatively charged; blue apolar; green polar; cyan Tyrosine and Histidine; Glycine orange; Cysteine pink and Proline yellow). Red dots indicate the positions of experimental mutations noted in the main text. Blue labels reference major secondary structure elements.

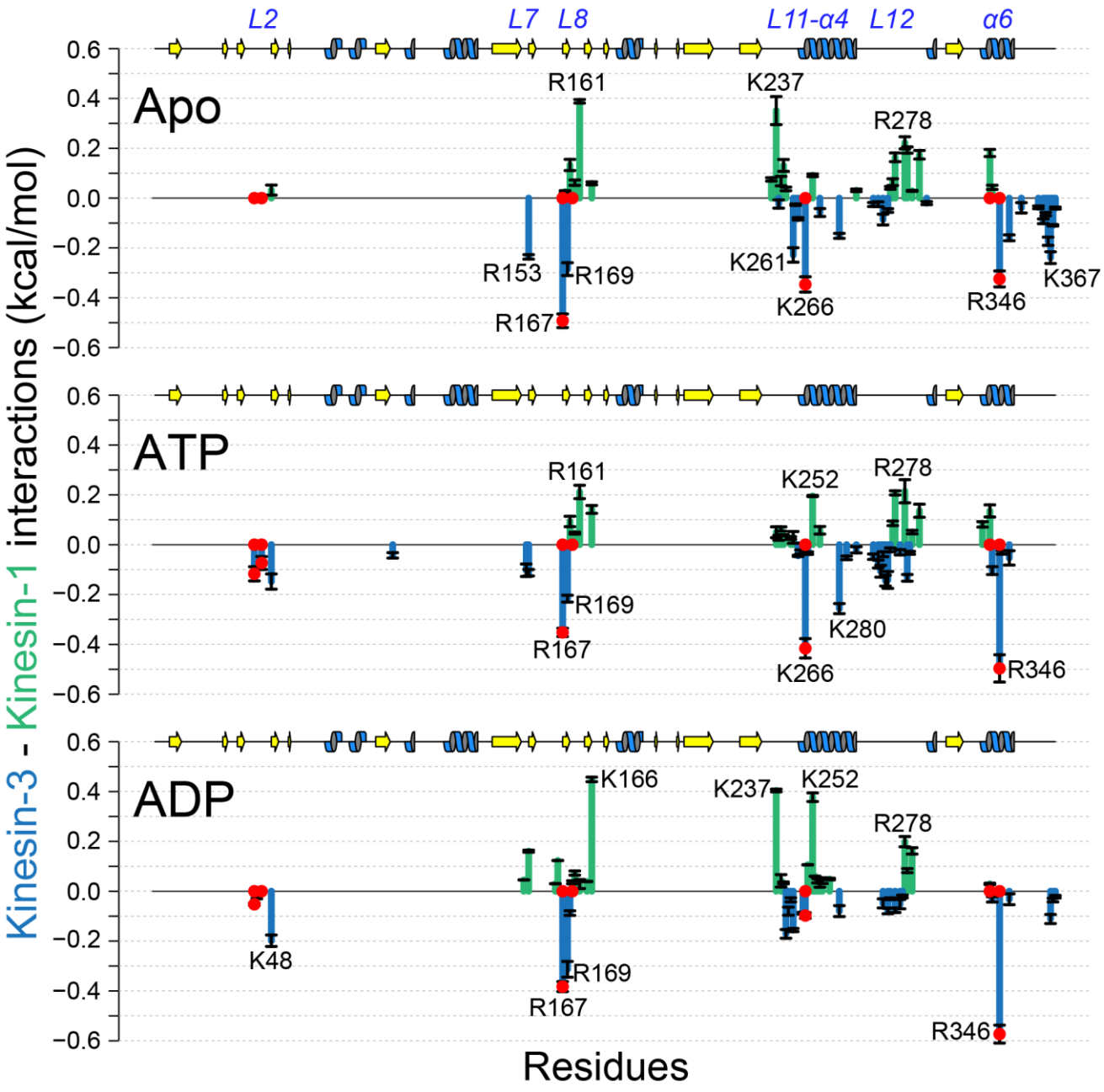

Figure S5. Differences in residue contribution to binding energy for kinesin-1 (green) and kinesin-3 (blue) in the Apo, ATP and ADP states. These values were determined from 4 replicate 40ns molecular dynamics simulations and subsequent energetic calculations. The location of residues subjected to mutagenesis simulations and single molecule experiments are indicated with red points.

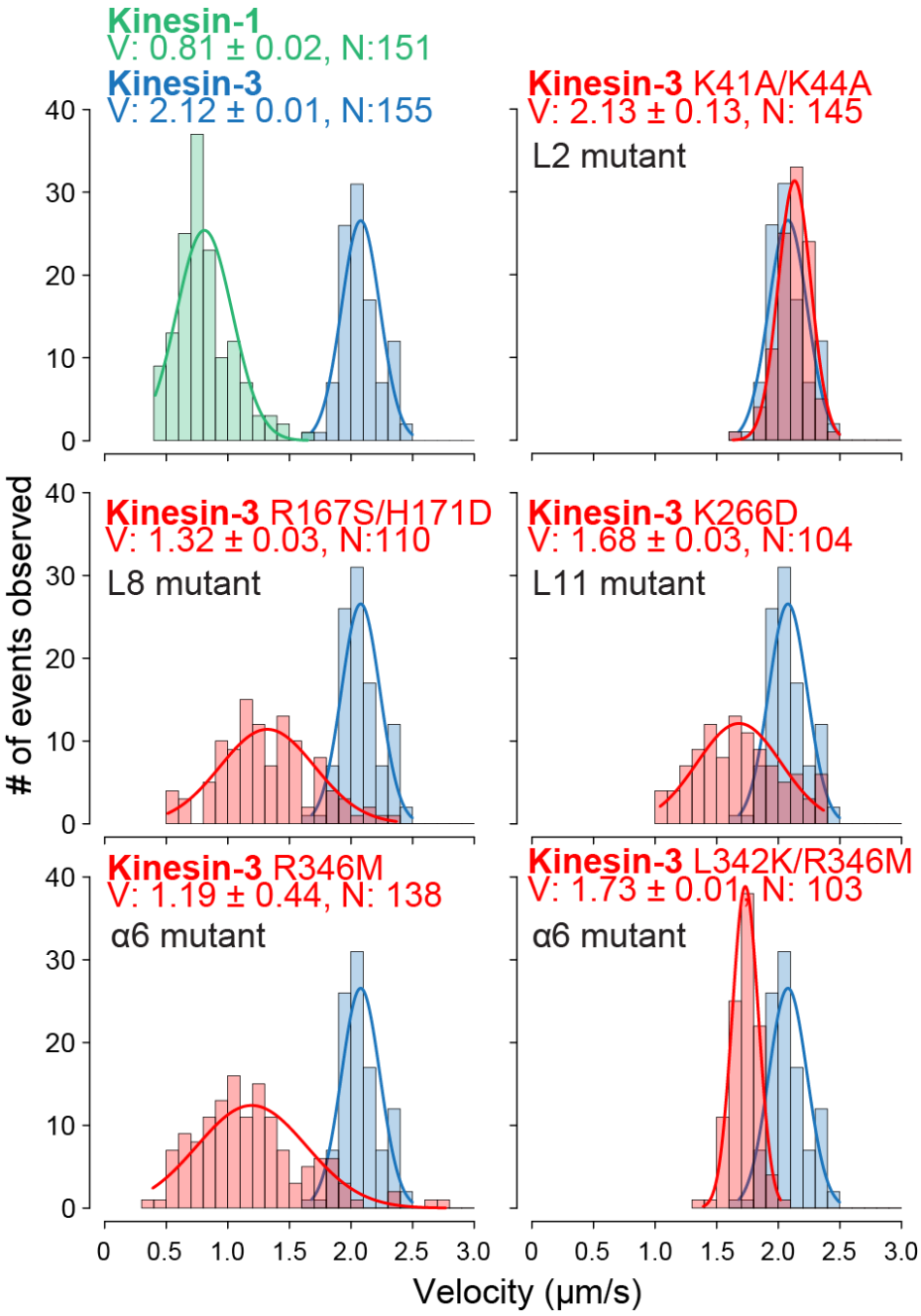

Figure S6. Experimental velocity measurements for kinesin-1 wild type, kinesin-3 wild type and kinesin-3 mutants.

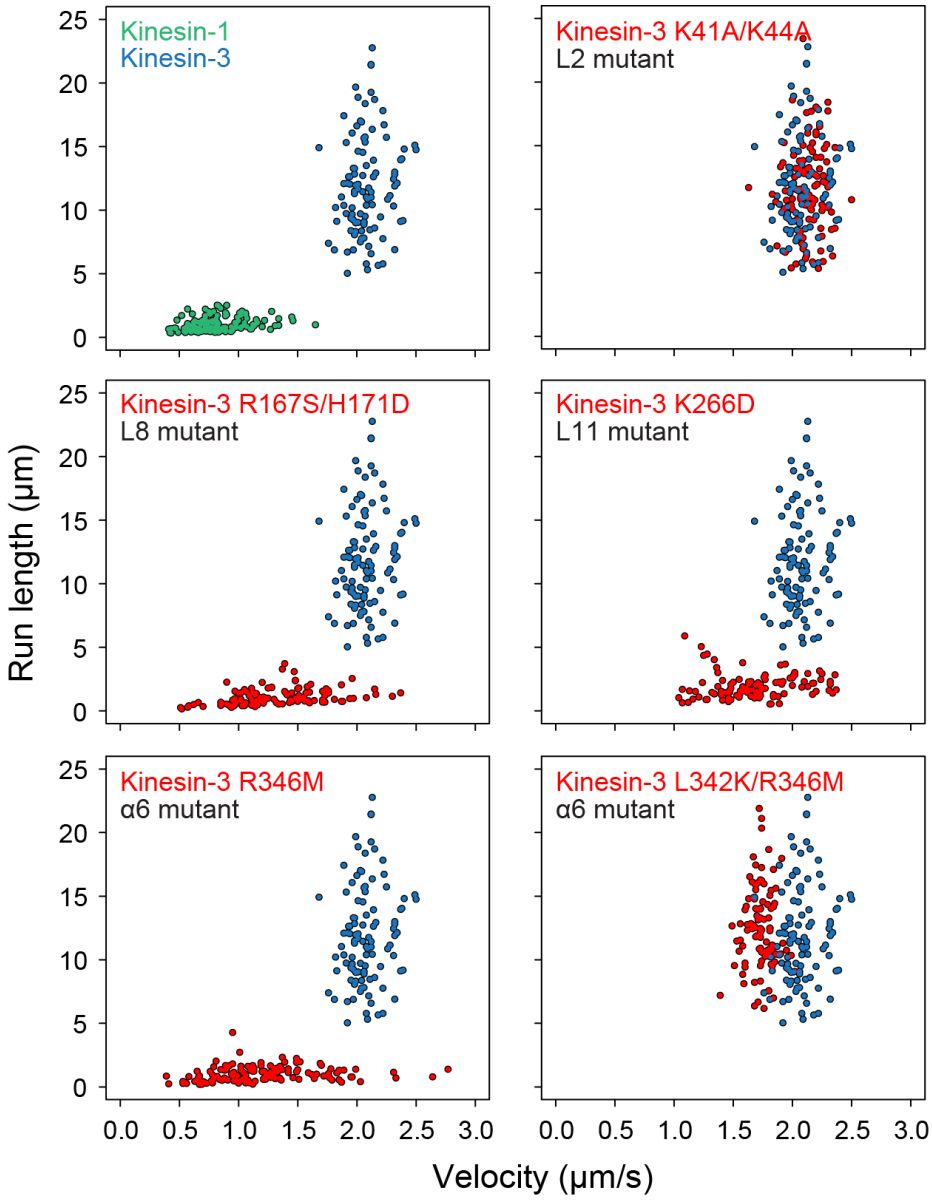

Figure S7. Experimental velocity versus Run length measurements for kinesin-1 wild type (green), kinesin-3 wild type (blue) and kinesin-3 mutants (red).

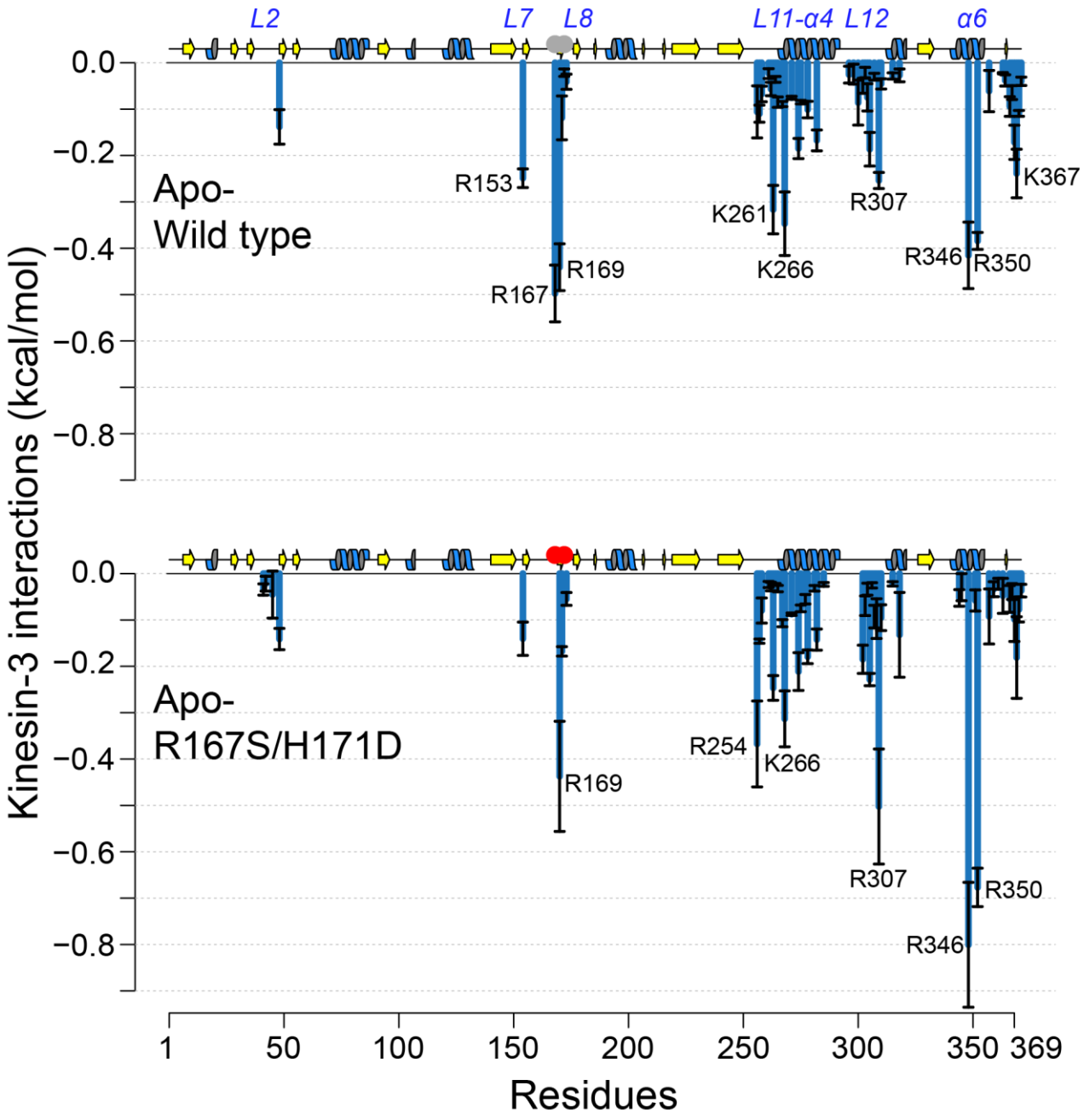

Figure S8. Results for the kinesin-3 L8 double mutant R167S/H171D in the Apo state. Kinesin residues with prominent contributions are labeled in black. The mutation sites are indicated with gray points in the WT plot and with red points in the L8 mutant plot. Note the absence of contributions from position 167 in the mutant but enhanced contributions from R307, R346 and R350.